Cellular automata model of gravity-driven granular flows

Keirnan R. LaMarche · **Stephen L. Conway** ·
Benjamin J. Glasser · **Troy Shinbrot**

Abstract   A cellular automata model is used to simulate a variety of granular chute flows. The model is tested against several case studies: flow down a chute, flow past an obstacle, chute flow in which complex, counter-rotating vortices result in streamwise surface stripes and flow near a boundary. The model successfully reproduces experimental observations in all of these cases. These results lead us to propose that simple, rule-based, models such as this can improve our detailed understanding of dynamics and flow within an opaque granular bed.

1 Introduction

Granular flows are an important part of many industrial and geophysical processes [1,2]. Even though granular flows are broadly important, the mechanistic understanding of their behaviors is limited. These behaviors are often complex and difficult to predict, and although good models have been produced for extremes of flow

K. R. LaMarche · S. L. Conway · B. J. Glasser
Department of Chemical & Biochemical Engineering,
Rutgers University, Piscataway, NJ 08854, USA

T. Shinbrot (✉)
Department of Biomedical Engineering, Rutgers University,
Piscataway, NJ 08854, USA
e-mail: shinbrot@soemail.rutgers.edu

Present Address:
S. L. Conway
Merck & Co., Inc.,
Whitehouse Station, NJ 08889, USA

ranging from entirely quasi-static [3–5] to entirely rapid [6,7], no reliable model spanning this range exists.

In this paper, we attempt to elucidate some of the qualitative rules of behavior that apply to granular flows ranging from static to freely flowing. We do so by focusing on a single archetypal geometry: flow down an inclined plane. This geometry is widely used in practical transport— for example in mining and manufacturing— and is seen in geological avalanching flows [8,9].

A promising development in understanding these static-flow transitions in granular beds was introduced in 1994 by a collaboration of authors with the acronym: BCRE [10]. The BCRE model defines an interface between a flowing layer of grains and a solidified bed beneath, and permits the interface to move up or down so as to account for material transfer between the flowing and static regions. The BCRE model has great potential to permit the future analysis of flow transitions, but in its present form is limited insofar as it does not predict the rich variety of behaviors seen in flowing granular beds. As an example of this variety, Savage, in 1979, examined the flow of glass beads in chutes with both rough and smooth surfaces [11], and reported a transverse circulatory flow (cf. Fig. 5b) that appeared when surfaces were roughened, but were not present using smooth surfaces. Thus Savage introduced the idea that there is apparently an internal flow within the granular bed that can be provoked by external effects such as roughening. It is difficult to incorporate such complex internal flows within a formalism such as BCRE, in which the flowing layer's dynamics are prescribed by simple kinetic considerations.

More recently, the understanding of complex internal flows has been advanced by experiments and analysis by Forterre and Pouliquen [12], who studied longitudinal

and other vortices that appear in wide, rough-bottomed chutes. These vortices are orientated parallel to the mean flow direction and transport grains between the base of the chute and the free surface. Forterre and Pouliquen proposed that the rough surface of the chute caused particles near the bottom of the flow to be agitated by frequent collisions, and thereby to generate an increased local granular temperature and a decreased local density. Using kinetic theory modeling, Forterre and Pouliquen [13] further showed that chute flow on rough bottoms could indeed become unstable to transverse perturbations and would produce counter-rotating vortices.

In this paper, we seek to use a cellular automata model to capture the spirit of BCRE, which defines transitions between a flowing surface layer and an underlying static bed so that complex chute flows—including those with boundary instabilities—can be simulated.

2 Cellular automata for free surface granular flows

Cellular automata (CA) models are based on simple rules that govern the interactions of neighboring cells. These models have been applied to a variety of complex systems including those involved in turbulence, combustion, and bacterial growth [14,15]. In the granular flow literature, cellular automata have also had a long history, including applications to avalanches [16,17], sand pile creation [18], jamming [19], flow from a hopper [20,21], the segregation of particles in rotating drums [22,23], and other problems. Examples of simple CA models for both flow from a hopper and segregation in a rotating horizontal drum have been given by Savage [24]. As stated by Baxter and Behringer [20], cellular automata models have important advantages over the more widely used continuous and discrete element methods. Continuous models are limited to systems with both simple geometries and spherical particles. The constitutive relations for continuous models, which are necessary for accurate simulations, are still being developed. As for discrete element methods, they are limited by the computational cost of tracking large numbers of particles. Recent work by Bazant (2006) has tried to address the computational limitations of DEM while still capturing the important physics through a "spot model" [25]. A review of the many methods for modeling granular materials was written by Herrmann and Luding [26]. While there are limits to the predictive capabilities of CA models, they are much faster than alternatives, allowing larger and more complex systems to be studied.

In this section, we describe a CA that is motivated by the BCRE model, which permits an interface between a surface flowing layer of grains and a solidified bed beneath to move up or down so as to account for material transfer between flowing and static regions. Correspondingly, we construct our CA by permitting 'material' above an interface to flow downhill, and constraining material beneath the interface to remain fixed in place. The interface itself evolves dynamically according to prescribed rules—essentially, if the free surface of the simulated granular bed is steep, the interface will submerge (causing more material to flow), until the surface slope lessens, at which point the interface will rise (reducing or even halting the flow).

In detail, the chute is modeled as a discrete grid of points in X and Y, each with a continuous height, $Z(X,Y)$. Flow of material is simulated by transferring a quantity $\Delta Z(X,Y)$ in a downhill direction, where downhill is determined by a calculation of the gradient of Z. The gradient is calculated in the X-direction at the grid locations (X_i, Y_j) so that it always points downhill:

$$\nabla_{i,j}^X = (Z_{i,j} - Z_{i-1,j}) \quad \text{if} \quad Z_{i-1,j} < Z_{i,j}, \quad \text{or}$$
$$\nabla_{i,j}^X = (Z_{i,j} - Z_{i+1,j}) \quad \text{if} \quad Z_{i+1,j} < Z_{i,j}. \tag{1a}$$

Similarly in the Y-direction:

$$\nabla_{i,j}^Y = (Z_{i,j} - Z_{i,j-1}) \quad \text{if} \quad Z_{i,j-1} < Z_{i,j}, \quad \text{or}$$
$$\nabla_{i,j}^Y = (Z_{i,j} - Z_{i,j+1}) \quad \text{if} \quad Z_{i,j+1} < Z_{i,j}. \tag{1b}$$

If (X_i, Y_j) is a local maximum, the larger slope is chosen; if it is a local minimum or if both slopes happen to be the same, one is chosen at random.

At each time step an amount of height, ΔZ, proportional to the slope is removed from a point and the same ΔZ is added to the height of another point downhill a distance, again, proportional to the slope. In this way, the CA explicitly conserves volume: every quantity of material removed from one location is deposited in another, downhill, location:

$$Z_{i,j} \to Z_{i,j} - \alpha \left(\nabla_{i,j}^X + \nabla_{i,j}^Y \right) \quad \text{and}$$
$$Z_{i+k^X, j+k^Y} \to Z_{i+k^X, j+k^Y} + \alpha \left(\nabla_{i,j}^X + \nabla_{i,j}^Y \right). \tag{2}$$

The distances, k^X and k^Y, at which material is deposited are calculated to again be proportional to the local gradient:

$$k^X = k_{i,j}^X = \text{int} \left(\beta \nabla_{i,j}^X \right),$$
$$k^Y = k_{i,j}^Y = \text{int} \left(\beta \nabla_{i,j}^Y \right), \tag{3}$$

In these equations, α and β are constants: α defines how thick the flowing layer will be, and β defines how far it
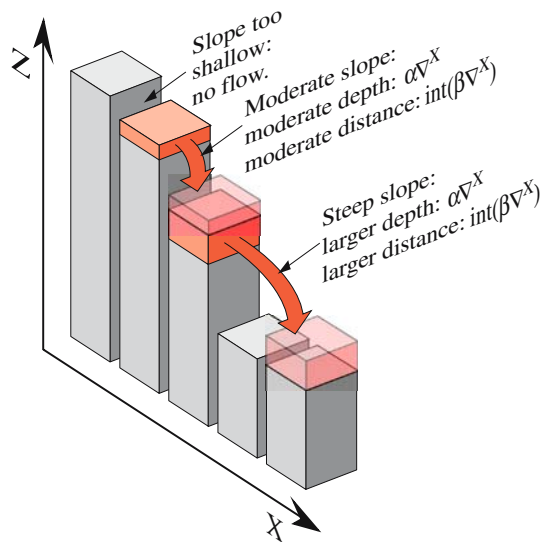
Fig. 1 Schematic of the flow of height in the CA model. The amount of height moved downhill and the distance that it is moved both depend on the slope, ∇^X. Here the case for the calculation in the x-direction is shown; a similar process is used for flow in the y-direction

will travel per unit time (i.e. its velocity). A schematic of this process is shown in Fig. 1.

We note that k^X and k^Y are necessarily integers, since the model surface is only defined at discrete X and Y gridpoints, so if k^X or k^Y is less than the grid spacing, no material will be transported in the corresponding direction. Thus for free the simulation provides an angle of repose, or gradient, below which flow will stop: this repose angle is defined such that whenever the total slope $\nabla_{i,j}^X + \nabla_{i,j}^Y$ decreases below $1/\beta$, flow stops. This is illustrated in Fig. 2, where we show the outcome of a simulation beginning with a sum of 5 random Fourier terms (i.e. sinusoidal shapes of random amplitude) in X and Y directions. Initially, some surface gradients, ∇, exceeded the angle of repose specified above, and so material (i.e. surface height) was transported to fill valleys downhill until the angle of repose was no longer exceeded. Consequently, in the histogram shown beneath the surface plot in Fig. 2, surface gradients reach a maximum critical amplitude; slopes below this amplitude are also present in valleys or near peaks. Parameter values used in this example are given in the figure caption.

In summary, this model prescribes simple flow in the spirit of the BCRE model: material beneath an interface (defined by $Z_{i,j} - \alpha \left(\nabla_{i,j}^X + \nabla_{i,j}^Y \right)$) is solid-like, while material above the interface travels with velocity int $\left(\beta \nabla_{i,j} \right)$ per unit time. The model is easily embellished by including terms to simulate diffusive, viscous, boundary, and body force effects. We describe such embellishments next.
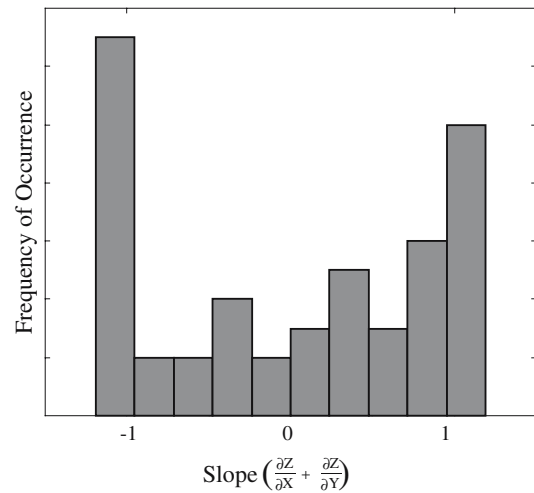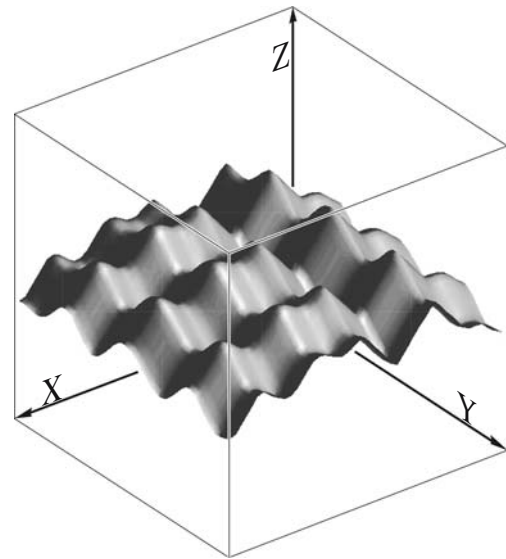
Fig. 2 *Top*: Surface shape simulated by cellular automata code beginning with 5 random amplitude Fourier modes in X and Y directions. Boundary conditions are periodic in X and Y, and the plot shown is a surface using a 50×50 grid, $\alpha = 0.01$, $\beta = 0.2$, and diffusion = 0.01. *Bottom*: Histogram of slopes for the surface shown above

2.1 Diffusion

To include diffusive motion of particles—either due to collisional effects in the moving layer or random wandering of particles near the surface—we add white noise of maximum amplitude δ to the gradient terms [27]. For either stalled or well developed flows, this typically has little effect; for near-critical flows (i.e. surfaces on the verge of motion as prescribed by Eq. (3)), this causes small variations similar to the motion of a single particle. These variations are observed to trigger subsequent avalanches of either small or large extent, depending on the states of nearby slopes [28].

2.2 Viscosity

Viscous memory can be added to the model by retaining a fraction of a point's previous velocity for the next time step. This is done by modifying Eq. (1) as follows:

$$\tilde{\nabla}_{i,j}^{X} = \nabla_{i,j}^{X} + (1 - \nu)\,\nabla_{-i,j}^{X}.$$
$$\tilde{\nabla}_{i,j}^{Y} = \nabla_{i,j}^{Y} + (1 - \nu)\,\nabla_{-i,j}^{Y}. \tag{4}$$

Here, $\tilde{\nabla}$ is the gradient corrected to include viscosity, ν, and ∇_{-} is the slope from the previous time step. The coefficient ν represents the effective viscosity and is chosen on [0, 1]: for small ν, the speed increases as the bed travels downhill, and when ν approaches 1, the bed responds only to the current slope. These two limits approximate the behaviors seen respectively in spherical beads with few collisions that can continually accelerate as they travel down a chute [29] and in small, highly dissipative, grains that rapidly acquire a terminal velocity [11].

2.3 Boundary conditions

The simplest boundary conditions that one can apply are periodic: thus in Fig. 2, all gradients and flows that travel off the rightmost edge of the simulation domain are calculated to continue at the leftmost edge, and similarly in front and back. Practical problems are not periodic, however, and so realistic boundary conditions are needed. Boundary conditions in granular systems are notoriously problematic [30]. For the X-direction boundary condition, a simple choice could be no-flux, and this can be specified by fixing gradients transverse to a wall to be zero, thus preventing any flow toward or away from a boundary. On the other hand, stress-free conditions in the cross-stream direction are approximated by reflecting any bed material leaving the domain, say in the $+X$-direction, back an equal distance in the $-X$-direction. The no-flux and no-stress conditions are appropriate for many cross-stream flows, but are not typically suitable in the streamwise direction, especially when convective, frictional or other influences occur near boundaries. Therefore we have included a variety of boundary alternatives in the CA (examples of some of these alternatives are shown in subsequent sections).

Taking Y to be the downstream coordinate, we can apply a fixed frictional momentum flux at the walls by decreasing the calculated slope at the wall in the Y-direction. This changes both the quantity (from Eq. (2)) and the speed (from Eq. (3)) at which material travels downstream near the boundaries.

The boundary condition at the upstream and downstream ends of the simulation can be set for several possible geometries to approximate the conditions seen in experiments. Thus a continual inflow can be specified by setting the gradient in the Y-direction at the upstream end of the geometry of interest to be a fixed positive value. Similarly, a continual outflow can be specified at the bottom of the chute by fixing the gradient in the Y-direction there to be another fixed value. Alternatively, free outflow can be chosen by setting the height at the end of the computational domain to a value such that to entire last row of the chute it will appear that the next point is at a height lower that itself. This allows material to fall off of a simulated chute or similar geometry without slowing down and impeding the flow behind it.

2.4 Vortices

For boundary conditions on the underside of a granular bed, we again provide alternative formulations. To model a smooth-bottomed surface, the slope is calculated and the height is moved in the direction of steepest downward slope as specified in Eqs. (1)–(3). Rough-bottomed chutes, on the other hand, are recognized to produce granular "heating" (an increase in mean fluctuational velocities) as grains collide with surface asperities [12], which then leads to the formation of three-dimensional (3D) vortices that transport high temperature grains to the surface while submerging lower temperature grains as the material flows downhill. In this 2-dimensional model, 3D vortices cannot be captured. However, it is of interest to see if changes in the governing rules in the cross-stream direction can capture the basic features of such a circulation. In experiments, it is observed that material circulates within adjacent vortices to produce surface crests and troughs. This leads to crests (troughs) where a pair of vortices forces materials away from (toward) the base. From the point of view of the surface, material seems to disappear from the troughs and to reappear at the crests. It is of interest to add a rule to approximate this movement of material on the surface in the cross-stream direction. This can be accomplished by changing the signs of the gradients defined in Eq. (1a). While we recognize that this is an oversimplification of the mechanics of the circulatory process, it has the virtue of capturing the qualitative kinetics needed to provoke a cross-stream instability in an algorithmically facile manner. Using this simple change in one rule allows us to turn cross-stream instabilities on or off. This has the effect of destabilizing cross-flows in a manner that is similar to that seen in experiments [12]: we discuss this case in a later section.

2.5 Body forces

The CA that we have described can accommodate body forces in a straightforward manner. Simple inclines can be defined by adding a constant term to the gradient in a prescribed direction. Thus to simulate an incline in the Y-direction by an angle ϑ, we would add a constant proportional to $g_0 = g \cdot \sin(\vartheta)$ to Eq. (1b). Inclines can also be modeled by setting a base height along the chute such that a constant gradient is created in the downstream direction. Material then simply travels downhill according to the algorithm already presented.

2.6 Chute inclination

To compare the angle of inclination of both the model and experimental chute, we define a parameter ϕ to be the ratio of the chute inclination to the angle at which the flow stalls. This allows us to compare the chute inclinations where various phenomena are observed relative to a common endpoint (e.g. the angle at which motion stops) in both experiments and CA model.

3 Case studies: increasing complexity

3.1 Case 1: Flow down a smooth-bottomed incline

The simplest situation that one would want to be able to model correctly is flow down a smooth chute without boundaries. This is a problem that has been well studied both experimentally and analytically [31]. We begin by examining two configurations that have previously been studied experimentally: first, flow down a featureless inclined chute, and second, flow down an inclined chute past a single triangular obstacle.

3.1.1 Case 1(a): Flow at increasing inclinations

By changing the angle of inclination in the CA model, several states can be produced, as shown in Fig. 3. These results have been observed using both methods described in previous sections to produce an incline. All other cases reported here use only the base height to produce an incline. For small inclination angles, the flow reaches the angle of repose and stops flowing. Once the angle of the chute reaches a critical angle, material begins to flow in a nearly steady fashion, with only small height fluctuations provided by the small diffusive term described previously; parameter values used are defined in the figure caption.

As the effective inclination (i.e. g_0) is increased, ripples appear on the free surface as shown in Fig. 3b.
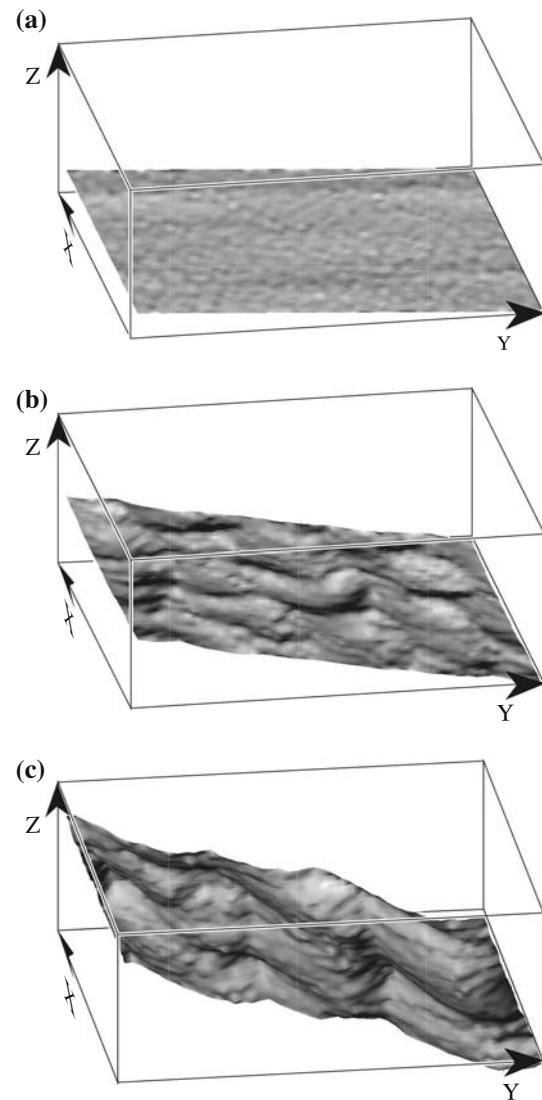
Fig. 3 Surface flows as the simulated angle of a smooth inclined chute is increased. **a** Smooth surface flow on a gently inclined chute ($g_o = 1$): here disturbances have time to disperse before additional material from uphill accumulates. **b** At a larger inclination ($g_o = 3$), small bumps grow because material cannot flow away downhill before new material arrives from uphill. **c** At still larger inclination ($g_o = 5$), bumps grow more rapidly, and travel upstream. In all cases, flow is from left to right, and periodic boundary conditions are applied in both X and Y. To add verisimilitude, an average inclination is added to the plot; in reality there is a constant gradient added in the $+Y$-direction, but to make the computational domain periodic, the left side of the plot is at the same height as the right side. Parameter values used are: $\alpha = 0.1$; $\nu = 0.8$; $\beta = 0.5$; $\delta = 0.1$

These ripples are nearly stationary in the Y-direction, but at still higher g_0, the ripples grow and travel uphill (i.e. to the left, in the $-Y$-direction). This is in agreement with observations of granular flows [32], and the mechanism for this has been long understood to be as follows [10]. Once a small bump appears on a smooth
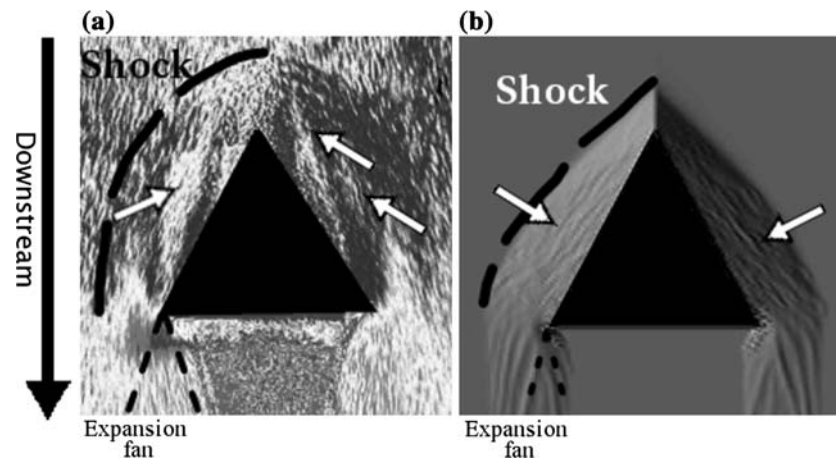
Fig. 4 Shockwaves produced **a** experimentally and **b** in CA in flow past a wedge. Experimentally and in the model, we identify the shock as the location where the bed depth increases abruptly. The expansion fan location is approximate. The experiments were carried out at $\phi = 1.24 \pm 0.01$ while the simulation angle was set to $\phi = 1.09$ (ϕ is defined in section 2.6). As can be seen in both figures, the shock waves are detached from the wedges, and the waves between the shock and the wedge have been marked with arrows. The experimental figure has been digitally enhanced to accentuate the waves. The black triangle denotes the position of the triangular wedge. The simulation was carried out on a 200 by 200 grid for 5,000 iterations with $\alpha = 0.04$, $\beta = 0.07$, $v = 0.565$ and no diffusion. The inlet boundary condition was set to a constant depth of 10

surface, material from uphill collides with the bump and slows. When this material reaches the trailing edge of the bump, it accelerates again under the influence of gravity, but not before more material has been accreted onto the leading, uphill, edge of the bump. If the mass flow rate of grains is small enough, the slowed material will have time to accelerate before more material arrives from uphill: in this case, the bump will flow downhill and diminish. On the other hand, if the incoming mass flow is above a critical threshold, more material will arrive from above than will be depleted from below, and the bump will move uphill and grow. This behavior is known to be associated with shock formation [33] and is reproduced in our CA model as a natural consequence of the explicit mass conservation specified by Eq. (1) combined with the flow models of Eqs. (1) and (3). We emphasize that this behavior is merely an elementary consequence of mass conservation, and does not imply that the CA model correctly approximates momentum conservation of granular flows. We therefore turn to more complicated situations to assess the degree to which the CA does, and at times does not, accurately reproduce realistic granular flows.

3.1.2 Case 1(b): Flow past an obstacle

Granular flow past obstacles has been studied using a variety of approaches. Rericha et al. [34] studied two-dimensional shockwaves past wedges using experiments, molecular dynamics simulations, and a continuum model. In that work, it was reported that shocks form at the leading edge of the wedge and an expansion fan forms at its base. Experimental examples of these features can be seen in Fig. 4a. Gray et al. [35] used pyramids to study supersonic avalanches around proposed barriers to rock slides and snow avalanches. In that work, experiments were compared with a simple hydraulic theory, using both forward- and backward-facing pyramids. Caram and Hong [36], by comparison, showed that simple random flow on a discrete lattice results in good agreement with experiments of granular flows past an obstacle.

In light of this pre-existing work, flow past an obstacle seems an appropriate candidate against which to test our CA model. Fig. 4b shows the simulated flow of material around a triangular wedge. The flow contains both a bow wave at the top of the wedge and an expansion fan at the base. Similarly when a pyramidal shape was placed into the flow, similar shockwaves to those of Gray et al. [35] were seen.

As shown in Fig. 4b, the shock produced by the model is detached from the wedge. Waves can also be seen within the shock, which are marked with arrows in that figure. To the best of our knowledge, these features have not been reported before in the literature on free surface granular flow around obstacles. However, when experiments were performed in our laboratory, similar detached shocks were observed, as can be seen in Fig. 4a. These shock waves are also detached from the obstacle and include internal waves propagating from the surface of the obstacle.
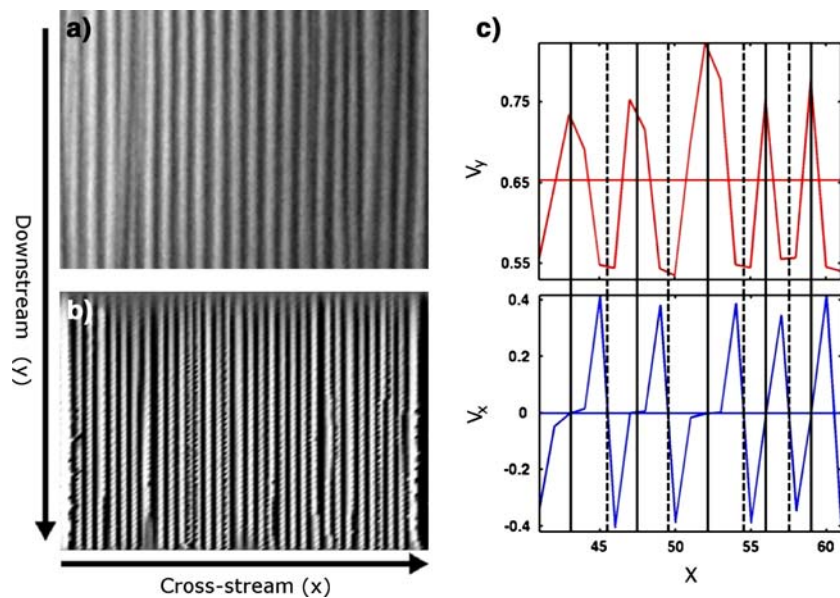
Fig. 5 Comparison of experimental longitudinal vortices (*above*) from Forterre and Pouliquen, and model CA vortices (*below*). **a** Picture of experimental stripes seen in a flow down a rough bed by Forterre and Pouliquen [12]. Experimental snapshot provided by Dr. Yoël Forterre. **b** Stripes produced by model with $\phi = 1.01$ on a 141 by 100 grid with $\alpha = 0.04$, $\beta = 0.07$, $\nu = 0.565$ for 1,500 iterations. Noise in the system caused by the rough bed was modeled using a high level of diffusion ($\delta = 10$). Other randomizing mechanisms were tested and produced similar results.

c Typical Streamwise (top) and spanwise (bottom) velocities from CA. Solid lines denote velocities at the crests while dashed lines denote velocities at the troughs. To produce the velocity profiles of the simulation the change in positions was averaged at each time step for each column of gridpoints along the longitudinal direction of the chute at $\phi = 1.01$. Simulations used for the velocity profiles were carried out on a 75 by 75 grid for 2,000 iterations while averaging for the final 500 iterations and with $\alpha = 0.04$, $\beta = 0.07$, $\nu = 0.565$ and $\delta = 10$

The experimental setup was similar to that of Conway et al. [37], consisting of an inclined acrylic sheet fed by a metal hopper. Sand with a diameter of $200 \pm 50\,\mu m$ was poured down the chute from the hopper. A wooden wedge was used as the obstacle, and was fixed to the center of the chute.

The detached shock wave and the waves within the shock were only seen at transitional flow speeds. The model displays subsonic behavior at low ϕ (below 1.08), which is followed by this translational behavior as ϕ is increased. At higher ϕ (above 1.13), the simulated shockwaves are no longer detached from the wedge. We have confirmed that this behavior is also found in experiments. Experimentally, below roughly $\phi = 1.14$, the flow is subsonic; above about 1.32, the flow appears to be supersonic (e.g. has upward traveling shocks), and between these points, the behavior of the flow seems similar to the transitional behavior of the CA model.

3.2 Case 2: Flow on a rough chute without sidewalls

A more complex flow recently described in wide, rough-bottomed chutes by Forterre and Pouliquen [12] consists of long streamwise undulations on the surface of the flow. Those authors provide convincing evidence that the patterns they observe, which they refer to as

longitudinal vortices, are created by granular heating at the rough surface. As the bed of grains travels down the chute, the velocities of those grains near the rough surface are randomized, leading to an increase in the granular temperature and a decrease in its density. This leads to a density inversion, in which a dense region sits on top of a less dense layer. This situation is unstable and causes the creation of longitudinal vortices. In order to model these three-dimensional vortices, the CA requires a similar unstable configuration. As described previously, this is produced by changing the sign of the gradient in Eq. (1a).

When many vortices are nucleated on the chute at the same time, they produce straight regularly spaced stripes. This nucleation can be accomplished by adding a random factor to the velocities of the flowing height for a number of iterations. This is similar to the randomizing effect of a rough-bottomed chute. Indeed, adding a random factor to the minimum chute height, or a random entrance boundary condition has a similar effect. The surface shapes thus produced are shown in Fig. 5, and seem to outwardly resemble the longitudinal vortices reported by Forterre and Pouliquen [12].

The velocity profiles of the experiments and model can be compared in greater detail. By averaging the distance material travels every timestep along each

streamwise column of grid points, a velocity profile can be obtained. Like the velocity profile reported by Forterre and Pouliquen, the streamwise velocity obtained from our CA model is slowest in the crests of the vortices and fastest in the troughs (see Fig. 5c). The velocity profiles are also similar in the cross-stream direction. As one expects for a vortical flow, the spanwise velocity vanishes at extrema of streamwise velocities. However, the direction of the flow is reversed in the CA model as a consequence of the algorithmic approximation, described previously, by which we generated the vortical instability. In experiments, material surfaces on the crests and is transported to the troughs where it is submerged and transferred back to the crests. In the CA model, this transport is projected onto a two-dimensional flow. Material is conveyed to the crests where it "jumps" and is carried to the troughs. This leads to a reversal in the directions of the velocity in the cross-stream direction.

3.3 Case 3: Flow on a smooth chute with rough sidewalls

More complex three-dimensional surface waves have been reported in inclined channels near frictional boundaries [37]. As shown in Fig. 6a, a granular bed flowing on a smooth surface with *roughened* sidewalls develops chevron-shaped free surface waves. Chevrons are seen experimentally at chute inclinations between 24° and 32°. These may constitute an analogy with fluid boundary layer flows, in which phenomena such as hairpin vortices develop near boundaries, signifying the onset of turbulence [38].

These patterns provide another test of the CA model's ability to simulate instabilities. Like the longitudinal vortices, the instabilities must be nucleated: in this case they are nucleated at the wall of the chute by creating disturbances in the amount of material near the wall. A no-slip condition is also set at the edge of the chute. These disturbances perturb the unstable bed and lead to the formation of vortices that behave, at least qualitatively, in much the same way as experimentally observed chevrons, as can be seen in Fig. 6b.

It has been proposed [37] that granular heating occurs at the walls and this creates vortices. The original chevron experiments [37] also reported streamwise circulatory flow in which grains beneath the surface flow away from the walls. We point out that the source of the orientation of experimental chevrons remains unclear. That is, if a vortical disturbance similar to that seen in Fig. 6 were produced near the sidewalls of a chute, one would naively expect any incipient vortices to be dragged downhill by the faster flow nearer the chute
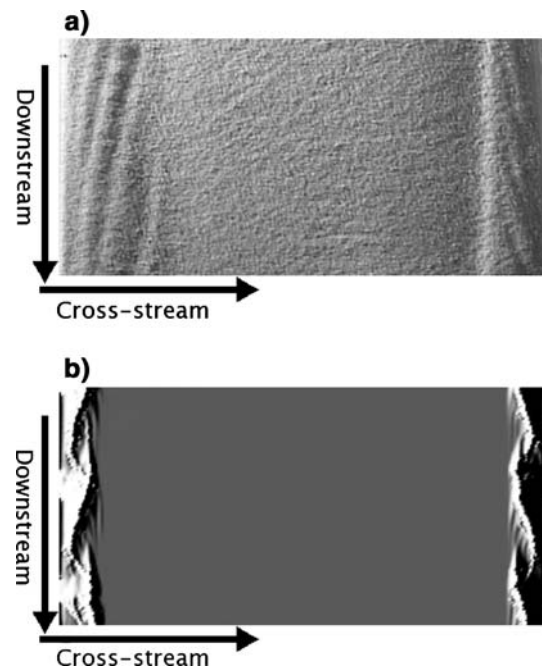
Fig. 6 Comparison of experimental and model chevrons. **a** Experimentally observed chevrons for $\phi = 1.04 \pm 0.01$. **b** Chevrons produced in model for $\phi = 1.05$ with no slip boundary conditions. The simulation was performed with a gridsize of 310 by 200 for 500 iterations. Here $\alpha = 0.04$, $\beta = 0.07$, $\nu = 0.565$, with no diffusion. The inlet boundary condition was set to a constant height of 10 while the depth of the bed was set to 50 for the initial condition except for three initially reduced height sections along each wall to perturb the bed

center. This would produce downward, V-shaped, chevrons, rather than the upward, Λ-shaped, ones that actually appear. It is therefore somewhat surprising that CA reproduces the correct chevron orientation, against simple heuristic expectations.

The dynamic behavior of the chevrons is at least qualitatively reproduced in the simulations. It was observed that both the angle of the chevron to the wall decreased over time and the distance between each chevron and the edge of the chute *increased* over time. The ultimate result of these combined effects is that convection rolls begin close to the side of the chute, at a large angle, and move away from the wall, while approaching a parallel orientation to the wall. This behavior has been observed in both simulations and experiments. A comparison between time-lapse snapshots from both simulations and experiments is shown in Fig. 7.

4 Other phenomena

This cellular automata model also seems to recreate other patterns observed in experiments. Forterre and

Fig. 7 Chevron angle change in both experiments and model: elapsed time is from top to bottom. **a** Time progression of a chevron from computational simulations at 7,500, 12,300 and 17,300 iterations. The angle of the chevron with the edge of the chute (dashed lines) is 9.5°, 6.0°, and 2.8° ± 0.3° respectively. Here $\phi = 1.01$, $\alpha = 0.04$, $\beta = 0.07$ and $\nu = 0.565$. **b** Experimental chevron at 1.3, 1.93, and 2.8 s with $\phi = 1.06 \pm 0.01$. The chevron's angle with the wall is 7.3°, 5.0° and 3.8° ± 0.3°, respectively. Cross-hatched areas indicate locations of the side-wall in both simulations and experiments
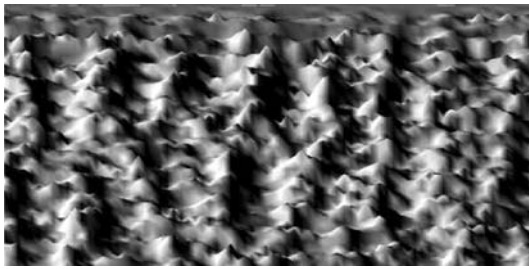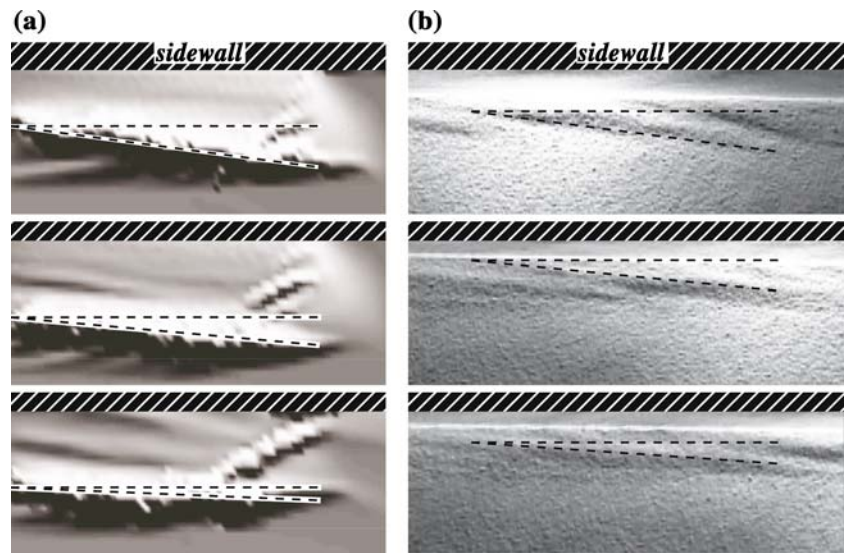
Fig. 8 Other phenomena: model scales. Both the experimental scales and these patterns are created at high chute angles. The experiments were reported at $\theta = 52°$ (see [13, Fig. 13]) whereas the model produced these features at $\phi = 1.16$. Here simulations were carried out on a 75 by 75 grid with $\alpha = 0.04$, $\beta = 0.07$, $\nu = 0.565$, and no diffusion

Pouliquen [13] have reported "scales" which appear in rough-bottomed chutes at high angles (52°). Similar structures form at high chute angles in the model. There is not a great deal of information available on these experimental structures. However, in both experiment and simulation, the structures tend to align themselves in both a streamwise and cross-stream lattice as can be seen in Fig. 8.

5 Conclusions

A very simple two-dimensional cellular automata model has been created to simulate the flow of granular materials in a chute. These simulations are limited by the two-dimensional nature of the calculations and a difficulty in determining a priori values for the physical parameters used. For example, the application of too much dissipation can lead to a state with no instabilities or to a frozen state. Too little dissipation results in patterns persisting in the model that would otherwise die out, or in the entire flow becoming unstable. Also, since the CA only models the 2D surface, subsurface flows, of granular materials cannot be examined. For example, the velocity profile of material below the surface cannot be captured. Thus the model cannot distinguish between flows down inclined planes—where the entire bed is in motion — and flows down piles of grains—where only the uppermost layers of grains are in motion.

Flow around obstacles was modeled and both sub- and super-sonic behaviors are qualitatively reproduced. A transitional region for a flowing free surface was observed for the first time in the model, and behaviors in this regime were qualitatively verified experimentally. This region is characterized by a detached bow wave within which other waves propagate from the surface of the obstacle. At higher inclination angles, near the upper end of the transition region, the model reproduces unstable 'scales' similar to those reported experimentally [13].

Regular patterned flow instabilities were also modeled. If the bed is disturbed uniformly, striped patterns are created which appear similar to the longitudinal vortices reported by Forterre and Pouliquen [12]. When the velocity profiles of the model and experiments are compared, similar qualitative trends can be seen. The velocity of material is slowest at the crests and fastest in the troughs [39] in the downstream direction while the velocity profile for the cross-stream direction is reversed for the model as compared with experiments.

Chevrons, another pattern created by unstable flow, are also examined. When disturbances are created near walls with a no-slip boundary condition, waves are created that are oriented against the flow. The dynamic behavior of both the experimental and model chevrons are similar.

While this simple model produces features that appear similar to some of the experimental patterns seen in chute flow, there are some important shortcomings that should be emphasized. Foremost, the CA model is only an approximate treatment and cannot be used to make accurate quantitative predictions using physical parameter values. Additionally, the model only provides a two-dimensional representation of three-dimensional phenomena. More careful scrutiny reveals additional differences between experiment and simulation. For example, as can be seen in Fig. 7, the chevrons in the model have sharper peaks than in experiments. This is due to issues associated with the choice of a value for dissipation in the model. This problem also plays a role in the long-term behavior of the model chevrons. In experiments, as the chevrons move toward the center of the chute, they transport material and deposit it at the point at which they are subsumed. Due to the difficulties in choosing an accurate value for the dissipation, at higher inclination angles, the vortices do not die out as they leave the edge of the chute, but instead join together and persist for long times.

In further detail still, experimentally two types of chevrons have been observed. Referred to as A and B chevrons [37], they differ in size and angle with respect to the wall. In the model, only one type of chevron is created. The mechanism that produces the A and B chevrons in the experiments at different chute angles is evidently not included in the cellular automata rules chosen for this model. Also, in experiments, chevrons and the longitudinal vortices of Pouliquen and Forterre are seen at very different chute angles. The chevrons are only seen for very low angles (about 25°), while the longitudinal vortices are seen at higher angles (about 40°) [12]. This discrepancy is not surprising considering that the model produces vortices regardless of the granular temperature, whereas in the experiments, it is the difference in granular temperature that drives the vortices.

For each flow feature modeled, boundary conditions or flow rules must be adjusted, especially when changing from smooth flow to the unstable flow of the density inversion patterns. Ideally a model with one set of flow rules would be able to capture all of these behaviors. Perhaps a three dimensional CA model may have more success in that regard. Nevertheless, this simple 2D model seems to capture qualitative experimental features quickly and efficiently and we hope may contribute to improved understanding of boundary conditions and dissipation rates which are appropriate for the wide range of granular behaviors currently being explored.

References

1. Knowlton, T.M., Carson, J.W., Klinzing, G.E., Yang, W.C.: Chem. Eng. Prog. **90**, 44 (1994)
2. Jaeger, H.M., Nagel, S.R., Behringer, R.P.: Rev. Mod. Phys. **68**, 1259 (1996)
3. Savage, S.B.: J. Fluid Mech. **377**, 1 (1998)
4. Pouliquen, O., Chevoir, F., Physique, C.R.: **3**, 163 (2002)
5. Bocquet, L., Losert, W., Schalk, D., Lubensky, T.C., Gollub, J.P.: Phys. Rev. E **65**, 011307 (2002)
6. Goldhirsch, I.: Annu. Rev. Fluid Mech. **35**, 267 (2003)
7. Lun, C.K.K., Savage, S.B., Jeffrey, D.J., Chepurniy, N.: J. Fluid Mech. **140**, 223 (1984)
8. Melosh, H.J.: Nature **379**, 601 (1996)
9. Iverson, R.M.: Rev. Geophys. **35**, 245 (1997)
10. Bouchaud, J.P., Cates, M.E., Prakash, J.R., Edwards, S.F.: J. Phys. I (France) **4**, 1383 (1994)
11. Savage, S.B.: J. Fluid Mech. **92**, 53 (1979)
12. Forterre, Y., Pouliquen, O.: Phys. Rev. Lett. **86**, 5886 (2001)
13. Forterre, Y., Pouliquen, O.: J. Fluid Mech. **467**, 361 (2002)
14. Wolfram, S.: Theory and Applications of Cellular Automata. World Scientific, Singapore (1986)
15. Wolfram, S.: A New Kind of Science. Wolfram Media Inc., Champaign, IL (2002)
16. Bak, P., Tang, C., Wiesenfeld, K.: Phys. Rev. Lett. **59**, 381 (1987)
17. Nerone, N., Gabbanelli, S.: Granular Matt. **3**, 117 (2001)
18. Goles, E., González, G., Herrmann, H.J., Martínez, S.: Granular Matt. **1**, 137 (1998)
19. Nagel, K., Herrmann, H.J.: Physica A **199**, 254 (1993)
20. Baxter, G.W., Behringer, R.P.: Phys. Rev. A **42**, 1017 (1990)
21. Kozicki, J., Tejchman, J.: Granular Matt. **7**, 45 (2005)
22. Yanagita, T.: Phys. Rev. Lett. **82**, 3488 (1999)
23. Ktitarev, D.V., Wolf, D.E.: Granular Matt. **1**, 141 (1998)
24. Savage, S.B.: In Disorder and Granular Media. Bideau, D., Hansen, A. (eds.) Elsevier Science, Amsterdam (1993)
25. Bazant, M.Z.: Mech. Mater. **38**, 717 (2006)
26. Herrmann, H.J., Luding, S.: Continuum Mech. Thermodyn. **10**, 189 (1998)
27. Samson, L., Ippolito, I., Dippel, S., Batrouni, G.G.: In: Powders and Grains '97. Behringer, R.P., Jenkings, J.T. (eds.) Balkema, Rotterdam (1997)
28. Daerr, A., Douady, S.: Nature **399**, 241 (1999)
29. Schafer, J., Dippel, S., Wolf, D.E.: J. Phys. I (France) **6**, 5 (1996)
30. Jenkins, J.T.: in Granular Gases, T. Pöschel, S. Luding (eds.) Springer, Berlin (2001); Bourzutschky, M., Miller, J.: Phys. Rev. Lett. **74**, 2216 (1995)
31. Hanes, D.M., Walton, O.R.: Powder Technol. **109**, 133 (2000); Louge, M.Y., Keast, S.C.: Phys. Fluid. **13**, 1213 (2001); Savage, S.B. Hutter, K.: J. Fluid Mech. **199**, 177 (1989)
32. Pak, H.K., Behringer, R.P.: Phys. Rev. Lett. **71**, 1832 (1993)

33. Soleymani, A., Zamankhan, P., Polashenski, W.: Appl. Phys. Lett. **84**, 4409 (2004)
34. Rericha, E.C., Bizon, C., Shattuck, M.D., Swinney, H.L.: Phys. Rev. Lett. **88**, 014302 (2002)
35. Gray, J.M.N.T., Tai, Y.-C., Noelle, S.: J. Fluid Mech. **491**, 161 (2003)
36. Caram, H., Hong, D.C.: Phys. Rev. Lett. **67**, 828 (1991)
37. Conway, S.L., Goldfarb, D.J., Shinbrot, T., Glasser, B.J.: Phys. Rev. Lett. **90**, 074301 (2003)
38. Herbert, T.: Annu. Rev. Fluid Mech. **20**, 487 (1988)
39. Caicedo-Carvajal, C.E., Glasser, B.J., Shinbrot, T.: J. Fluid Mech. **556**, 253 (2006)